Available online at www.sciencedirect.com
ScienceDirect
Trans. Nonferrous Met. Soc. China 28(2018) 1504−1513
Transactions of Nonferrous Metals Society of China
www.tnmsc.cn

Hot tearing behaviors and in-situ thermal analysis of Mg−7Zn−*x*Cu−0.6Zr alloys

Zhi WANG[1], Ye ZHOU[1], Yi-zhou LI[1], Feng WANG[1], Zheng LIU[1], Ping-li MAO[1], Xiao-ping JIANG[2]

1. School of Materials Science and Engineering, Shenyang University of Technology, Shenyang 110870, China;
2. Wanfeng AUTO Holding Group, Shaoxing 312000, China

Received 26 April 2017; accepted 22 December 2017

Abstract: Thermal analysis was used to investigate the microstructural evolution of Mg−7Zn−*x*Cu−0.6Zr alloys during solidification. The effect of Cu content (0, 1, 2 and 3, mass fraction, %) on the hot tearing behavior of the Mg−7Zn−*x*Cu−0.6Zr alloys was investigated with a constrained rod casting (CRC) apparatus, equipped with a load sensor and a data acquisition system. The thermal analysis results of Mg−7Zn−*x*Cu−0.6Zr alloy revealed that the alloy consisted of two distinct phases: α-Mg and $MgZn_2$. Three distinct peaks were observed in the alloys with Cu addition, which were identified as α-Mg, MgZnCu and $MgZn_2$. In addition, the reaction temperature of α-Mg decreased and the reaction temperatures of $MgZn_2$ and MgZnCu increased as the Cu content increased. The experimental results of hot tearing demonstrated that the addition of Cu significantly reduced the hot tearing susceptibility (HTS) of Mg−7Zn−*x*Cu−0.6Zr alloys due to the higher eutectic temperature and the shorter solidification temperature region.
Key words: Mg−7Zn−*x*Cu−0.6Zr alloy; microstructure; solidification path; hot tearing susceptibility

1 Introduction

Magnesium alloys constitute the light metallic structural materials in the automotive and aerospace industries, which exhibit high specific strength and stiffness, as well as good castability [1]. Generally, more than 85% of magnesium alloy products are manufactured through casting. Hot tearing, also referred as hot cracking, is a commonly observed defect encountered during solidification. Also, it is a significantly severe defect, which deteriorates the mechanical properties and restricts the application of magnesium alloy castings. Hot tearing is frequently considered to be a result of inadequate compensation of melt flow under thermal stress during solidification. In certain experimental and industrial studies it was demonstrated that hot tearing occurred at the end of solidification, when the solid fraction was 85% to 95% and a continuous dendritic network formed [2,3]. Therefore, it was extremely important to study the solidification characteristics of alloys (such as microstructure evolution and solid fraction) through the in-situ thermal analysis method. In this work, thermal analysis was utilized to record the sample temperature variation with time during solidification, whereas consequently a curve of temperature variation as a function of time was plotted accordingly. From this curve, the thermal release, related to latent heat evolution during each phase transformation, could be detected. To discover the characteristic parameters of a certain transformation, such as the onset and end of transformation, the cooling curve and its derivative curves were considered. This procedure is known as computer-aided cooling curve analysis (CA-CCA) [4]. The CA-CCA is one of the most widely utilized characteristics for the alloy solidification investigation, as it can be operated on site and is suitable for commercial applications [5]. Moreover, compared with other methods such as DTA or DSC, the CA-CCA is sufficient for the non-equilibrium solidification investigation of industrial alloys [4]. To date, the CA-CCA method has been widely utilized in Al and Mg foundries [6−11]. Adversely, the solidification characteristics of Mg−Zn−Cu−Zr systems are still not reported.

In addition, hot tearing is one of the most important

Foundation item: Projects (51504153, 51571145) supported by the National Natural Science Foundation of China; Project (L2015397) supported by the General Project of Scientific Research of the Education Department of Liaoning Province, China
Corresponding author: Zhi WANG; Tel: +86-13591634456; E-mail: wangzhi8303@163.com
DOI: 10.1016/S1003-6326(18)64791-0

characteristics to evaluate the castability of Mg alloys. Hot tearing has been an extensively studied subject and many testing methods and computational models were developed [2,3,12,13]. Hot tearing susceptibility (HTS) of binary Mg−Zn alloys was investigated by ZHOU et al [14] through thermodynamic calculation and experimental methods. It was discovered that the solidus decreased and the freezing range of binary Mg−Zn alloys increased with Zn addition, which resulted in high hot tearing tendency. The relationship between HTS and Zn content demonstrated that the HTS reached its peak value at 1.5% Zn (mass fraction). In addition, the effect of Al on the HTS of Mg−Zn alloys was also investigated through the CRC method. It was found that the HTS of Mg−Zn alloys decreased with the addition of Al [3]. Recently, wrought Mg−Zn−RE (RE is rare earth) alloys are one of the most commonly applied alloys in the industry. In contrast, the addition of RE leads to the increase of cost and the production is complicated. Compared with RE elements such as Nd, Gd, Y and Ce, Cu is considered a cost-effective alloying element for Mg alloys. Recently, Mg−Zn−Cu alloys have been considered as extremely promising wrought magnesium alloys for practical applications. Compared with binary Mg−Zn alloys, ZHU et al [15], BUHA and OHKUBO [16] reported that the Mg−Zn−Cu alloys had good castability and excellent age-hardening response. The corresponding results indicated that the addition of Cu could increase the eutectic temperatures of as-cast Mg−Zn alloys and the Mg−Zn−Cu alloys could be solution-treated at high temperatures [15]. Regarding Mg−Zn−Cu alloys, the previous reports were mainly focused on the corresponding microstructure and mechanical properties. In contrast, investigations on the corresponding solidification behaviors and hot tearing were barely conducted. Therefore, in order to promote the industrial applications of Mg−Zn−Cu alloys further, it was necessary to understand the solidification pathways, the phase constituent and the HTS of these alloys.

In this work, the phases evolution and the HTS of Mg−7Zn−xCu−0.6Zr (x=0, 1, 2, 3) alloys were studied through CA-CCA and constrained rod casting (CRC) during solidification. The effects of solid fraction (f_{DCP}) and temperature (T_{DCP}) at the dendrite coherency point on HTS were investigated. The experimental data could contribute to the Cu addition optimization for the Mg−Zn alloys.

2 Experimental

2.1 Computer-aided cooling curve analysis (CA-CCA)

CA-CCA was performed based on the thermocouple method that was developed by BACKERUD et al [17]. The Mg−7Zn−xCu−0.6Zr (x=0, 1, 2, 3) alloys were melted in a graphite crucible by an electrical resistance furnace. Two K-type thermocouples were immersed in the melt from the top of the crucible at exactly the same depth. One thermocouple placed adjacent to the wall (accordingly, the temperature collected from this thermocouple was marked as T_w) and the other at the center (the temperature collected from this thermocouple was marked as T_c) of the crucible. The solidification temperatures were recorded with a high-speed data acquisition system, which was linked to a computer as schematically presented in Fig. 1 [4]. The analysis was repeated three times for each alloy to ensure the result reliability.

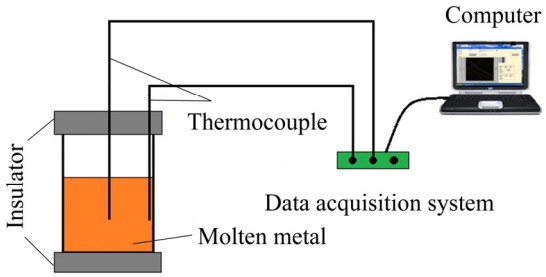

Fig. 1 Schematic diagram of CA-CCA setup [4]

2.2 Hot tearing tests

In the present study, the CRC apparatus with a load sensor was utilized to investigate the hot tearing initiation and propagation of Mg−7Zn−xCu−0.6Zr (x=0, 1, 2, 3) alloys, which was developed by ZHEN et al [18]. The apparatus consisted of a CRC mold, a load recording system and a data acquisition system, as shown in Fig. 2. The CRC mold consisted of a vertical sprue and a horizontal rod. A load sensor was connected to the horizontal rod end, which recorded the developed contraction force during solidification. The contraction force curve contributed to the information acquisition of hot tearing initiation. This information is very important to understand the mechanism of hot tearing. The apparatus details could be obtained from Ref. [18].

The nominal compositions of the studied alloys were Mg−7Zn−xCu−0.6Zr (x=0, 1, 2, 3). The alloy castings were produced through the CRC apparatus equipped with a load sensor and a data acquisition system. 350 g of the Mg alloy was melted in a cylindrical steel crucible at 700 °C, which was protected by high purity Ar+0.2%SF_6 mixed gas. The mold was coated with BN (hexagonal α-BN) to assist the melt flow. The mold was preheated to 250 °C. The hot tearing testing of each alloy was repeated at least three times, to ensure reproducibility of the result. The data recording of both the contraction force and temperature in the hot spot area was immediately activated by the computer once the casting started. These recorded experimental data were utilized for the hot tearing initiation information analysis,

such as the critical temperature. Following the ingot complete solidification, the hot cracking of the Mg−7Zn−xCu−0.6Zr (x=0, 1, 2, 3) alloys was observed and the macro-graphs were obtained with a digital camera.

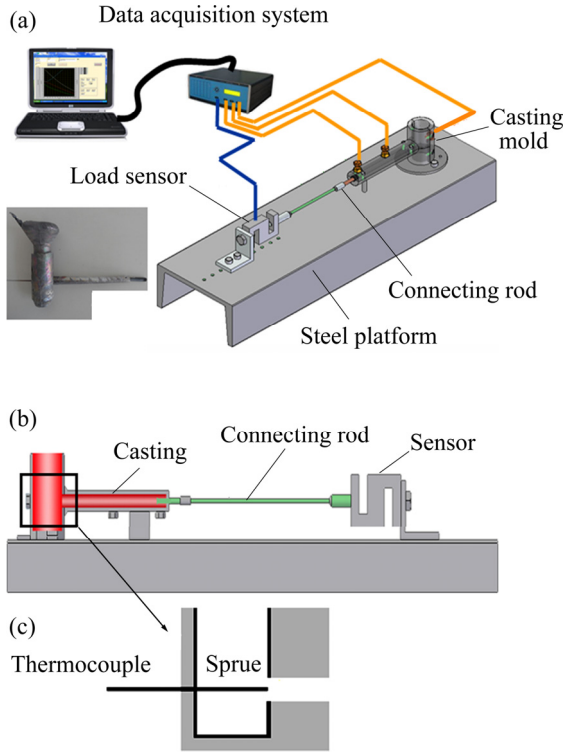

Fig. 2 Schematic of hot tearing tests setup: (a) Whole setup; (b) Device for detecting temperature and force during casting; (c) Thermocouple position for obtaining temperature at hot spot [18]

The HTS of the Mg−7Zn−xCu−0.6Zr (x=0, 1, 2, 3) alloys was evaluated according to the measurements of hot crack volumes through the wax penetration method. The method was simple and did not damage the samples. Subsequently, for the hot tearing experiments, the samples were cut from the sprue-horizontal rod junction in a T-shape, as well as immersed into a molten wax bath at 80 °C and retained for 10 min for temperature homogenization. Following, the bath was placed into a vacuum chamber for the air entrapped in the wax and inside the cracks to be removed. The vacuum valve was opened and a pressure of 0.1 MPa was immediately applied to the wax and the sample. With this pressure, the molten wax was injected into the cracks. Furthermore, the bath was cooled down and the solidified wax on the exterior surfaces of the sample was removed, while the wax inside the cracks was retained. The volume of the cracks can be determined through the following equation:

$$V_{cr}=\frac{m_2-m_1}{\rho_{wax}} \quad (1)$$

where V_{cr} is the volume of cracks; m_1 and m_2 are the masses of the magnesium casting sample prior to and following the injection of wax, respectively; ρ_{wax} is the paraffin wax density, ρ_{wax}=0.90 g/cm^3.

2.3 Microstructural analysis

The microstructures and hot tearing morphologies adjacent to the sprue-horizontal rod junction were studied with a scanning electron microscope (SEM). The samples were ground with different grades of SiC papers and consequently polished. Following polishing, these samples were chemically etched in a solution of 8 g of picric acid, 5 mL of acetic acid, 10 mL of distilled water and 100 mL of ethanol. The hot tearing fracture surfaces were observed with SEM.

The phase identification was performed with an X-ray diffractometer (Rikakn D/maxr) with Cu K_α radiation generated at 40 kV and 30 mA, as well as a scan rate of 4 (°)/min in a 2θ range of 20°−90°. According to the GB/T 13822−92 standard, the test samples originated from a horizontal rod of 10 mm in diameter and of 5 mm in height.

3 Experimental results

3.1 Phase identification

Figure 3 presents the constituent phases in the as-cast Mg−7Zn−xCu−0.6Zr (x=0, 1, 2, 3) alloys with various Cu contents, as obtained through X-ray diffraction. It could be observed that the Mg−7Zn−0.6Zr alloy mainly consisted of the α-Mg and $MgZn_2$ phases. As observed from Fig. 4(b), the white rod or dot-like phase was $MgZn_2$, which was located at the grain boundaries. In contrast, with Cu addition to the Mg−7Zn−0.6Zr alloys, the diffraction peaks of the MgZnCu phase were detected. The cubic MgZnCu phase was also confirmed through TEM examination at the grain boundaries [13]. The MgZnCu intermetallic compound was a Laves phase of the $C15$ $MgCu_2$ type

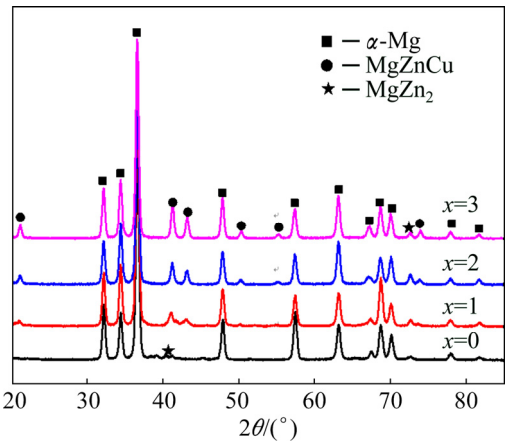

Fig. 3 XRD patterns of as-cast Mg−7Zn−xCu−0.6Zr alloys

which had high melting point and good thermal stability [19].

3.2 Computer-aided cooling curve analysis (CA-CCA)

Figure 4 shows the CA-CCA results and microstructures of the Mg−7Zn−*x*Cu−0.6Zr alloys. The cooling curve, the cooling gradient curve (d*T*/d*t*) and the baseline curves were included in these figures. These curves could be used to determine the thermal arrest points during solidification. The released latent heat could be arrested (arrest points on cooling curve) and related to the phase precipitation on the cooling curve. Therefore, the slope enhancement on the cooling gradient curves was related to the solidification reactions

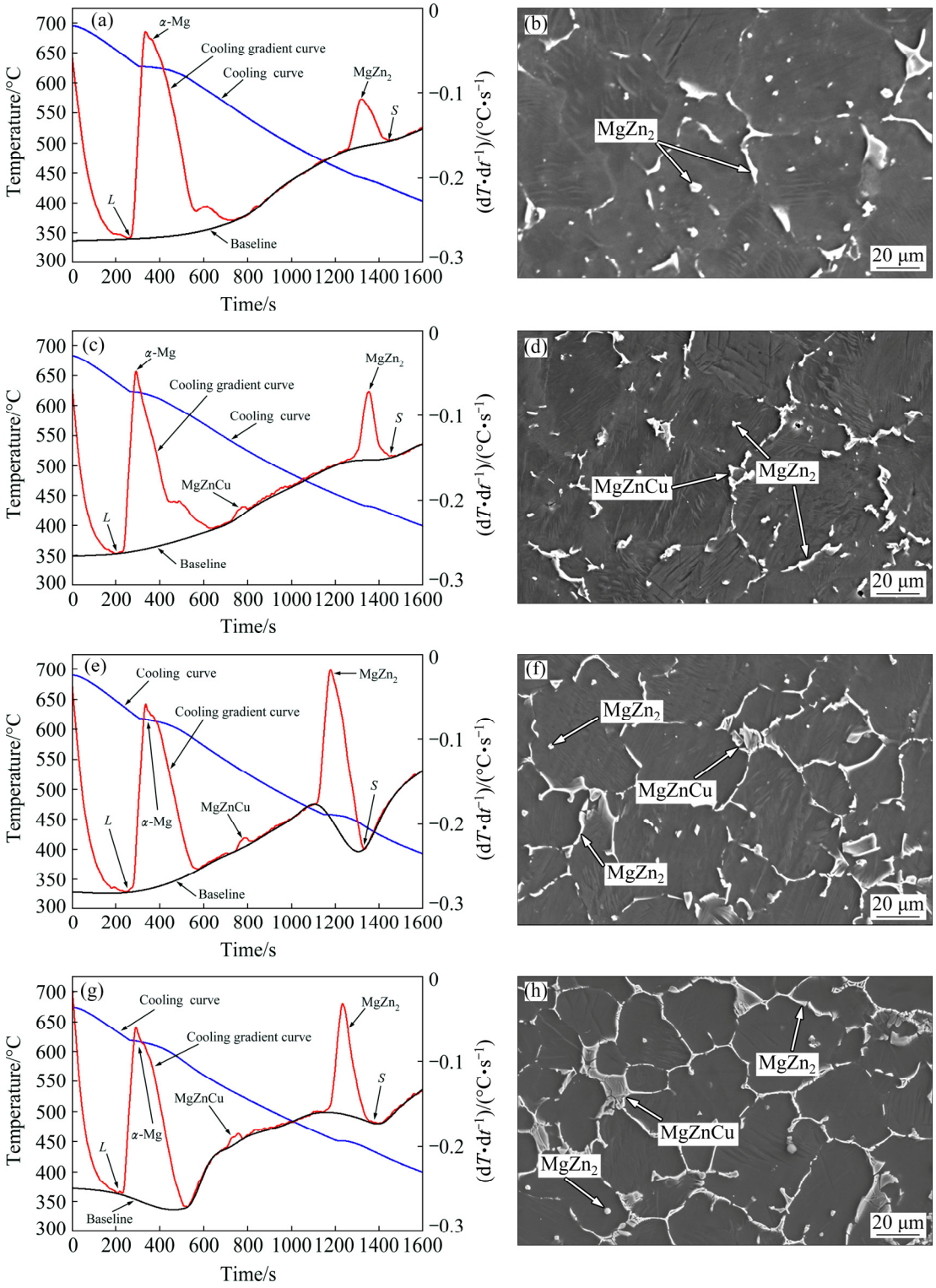

Fig. 4 CA-CCA results (a, c, e, g) and microstructures (b, d, f, h) of Mg−7Zn−*x*Cu−0.6Zr alloys: (a, b) *x*=0; (c, d) *x*=1; (e,f) *x*=2; (g, h) *x*=3

for different phases. These cooling gradient curves also facilitated the critical solidification conditions determination of these alloys. The baseline presented that no phase transformation existed during solidification. In order to obtain solid fraction during solidification, the baseline was fitted with the peak fitting square function, between the onset and the end of solidification. The solid fraction at each time frame included the area between the cooling gradient curve and the baseline. The solid fraction (f_s) can be given through the following equation [4]:

$$f_s = \frac{\int_{t_l}^{t}[(\mathrm{d}T/\mathrm{d}t)_{cc} - (\mathrm{d}T/\mathrm{d}t)_{bl}]\mathrm{d}t}{\int_{t_l}^{t_s}[(\mathrm{d}T/\mathrm{d}t)_{cc} - (\mathrm{d}T/\mathrm{d}t)_{bl}]\mathrm{d}t} \quad (2)$$

where subscripts "cc" and "bl" represent the cooling curve and the baseline, respectively; t_l is the time of start of solidification; t_s is the time of end of solidification; T is the solidification temperature; and t is the solidification time.

Regarding the Mg−7Zn−0.6Zr alloy, two apparent peaks existed in the dT/dt curve at 627 and 423 °C (Fig. 4(a)), respectively. These two peaks corresponded to the α-Mg phase formation and the non-equilibrium $L\rightarrow\alpha$-Mg+$MgZn_2$ eutectic reaction, according to the XRD analysis results. This was consistent with the microstructure observations, as presented in Fig. 4(b), where the eutectic structure of $MgZn_2$ was apparent within the α-Mg matrix. Three peaks were observed in XRD patterns of the Mg−7Zn−1Cu−0.6Zr alloy and occurred at the critical temperatures of 622, 531 and 432 °C, respectively (Fig. 4(c)). These peaks corresponded to the α-Mg precipitation, the MgZnCu phase formation and the non-equilibrium eutectic reaction ($L\rightarrow\alpha$-Mg+$MgZn_2$). From the microstructure observations, it could be observed that certain short rods, observed at the grain boundaries, were MgZnCu intermetallics, according to EDS analysis as denoted with an arrow in Fig. 4(d). The XRD analysis result, the microstructural observations and the CA-CCA results were in good agreement. The cooling and cooling gradient curves of the Mg−7Zn−2Cu−0.6Zr and Mg−7Zn−3Cu−0.6Zr alloys also presented similar peaks (Figs. 4(e) and (g)). Moreover, as shown in Figs. 4(f) and (h), the MgZnCu phase amount increased as the Cu content increased. The solidification path could be described as follows: The formation of α-Mg and MgZnCu led to the formation of $MgZn_2$ through the eutectic reaction.

All the phases for the Mg−7Zn−xCu−0.6Zr (x=0, 1, 2, 3) alloys were shown in Fig. 5 according to the CA-CCA results. It could be observed that the α-Mg precipitation temperature decreased from 627 to 616 °C as the Cu content increased from to 3% (mass fraction). In contrast, the $MgZn_2$ and MgZnCu precipitation temperatures increased as the Cu content increased. In addition, the formation temperature of $MgZn_2$ significantly increased by approximately 34 °C as the Cu content increased from 0 to 3%. Generally, the non-equilibrium eutectic temperature is defined as the solidification temperature end. In the case of Mg−7Zn−xCu−0.6Zr alloys, the formation temperature of $MgZn_2$ was considered as the end of solidification. It increased from 423 to 457 °C for both Mg−7Zn−0.6Zr and Mg−7Zn−3Cu−0.6Zr alloys.

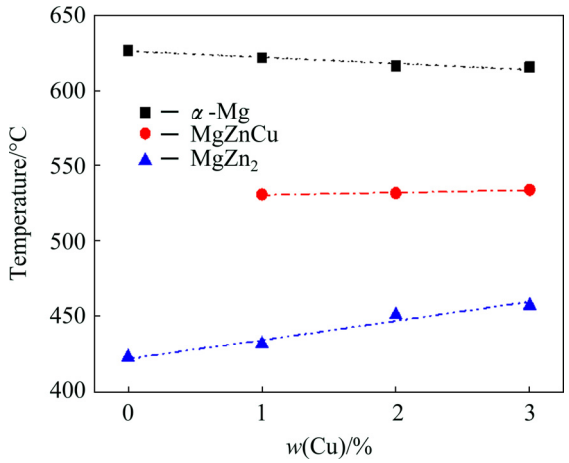

Fig. 5 Effect of Cu addition on CA-CCA results of Mg−7Zn−xCu−0.6Zr alloys

The data of dendrite coherency point (DCP) are a significantly important feature in the alloy solidification possesses, especially for the formation of casting defects, such as hot tearing [4]. The first maximum temperature difference between the center and the wall could be regarded as the DCP. Therefore, the coherency temperature and coherency time of the solidified dendrite could be obtained through the CA-CCA results (as shown in Fig. 6). The solid fraction at the DCP was calculated according to Eq. (1). Figure 7 presents the temperatures and solid fractions at the DCP of Mg−7Zn−xCu−0.6Zr alloys. It could be observed that the T_{DCP} decreased from 612 to 599 °C and the f_{DCP} increased from 28.3% to 43.7% as the Cu content increased from 0 to 3%.

3.3 Hot tearing susceptibility

Figure 8 shows the experimental curves of contraction force as a function of solidification time at the mold temperature of 250 °C for the as-cast Mg−7Zn−xCu−0.6Zr alloys. The information of hot tearing initiation and propagation could be obtained from the experimental curves, such as from the hot tearing initiation temperature (T_i) and hot tearing propagation stage. As shown in Fig. 8, the evolutions of contraction force were normally similar, but certain differences could

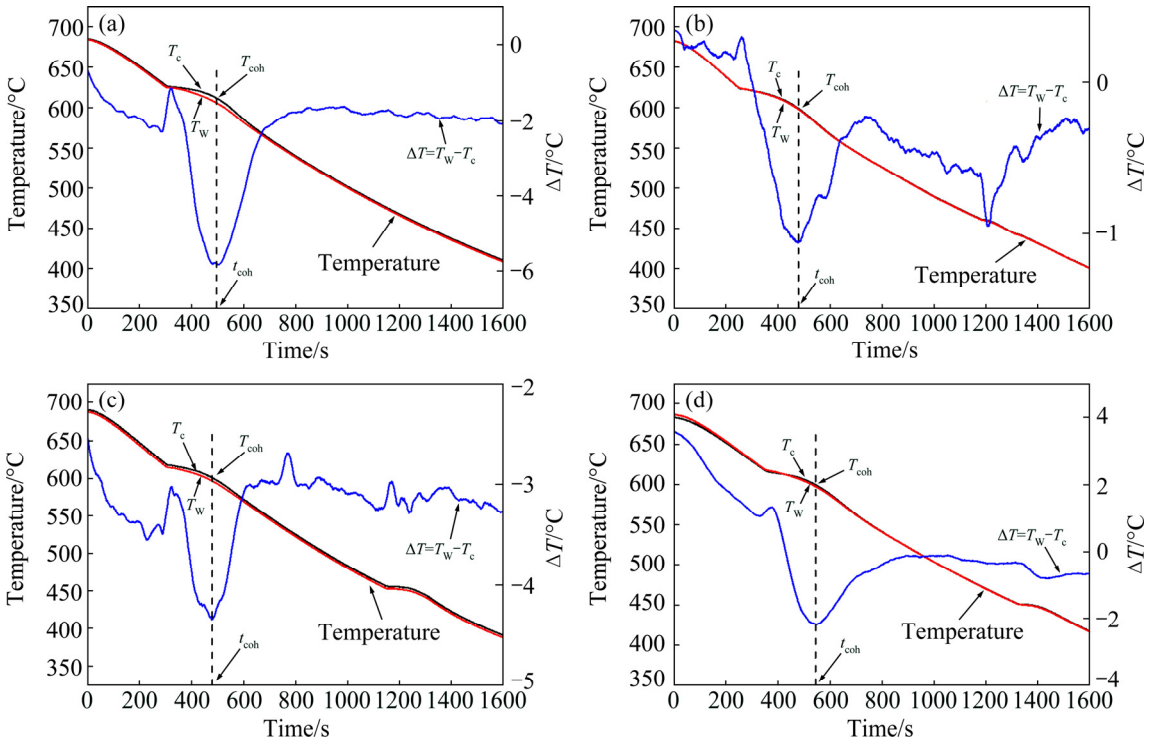

Fig. 6 Diagrams defining coherency temperature and time of solidified dendrite of Mg−7Zn−*x*Cu−0.6Zr alloys (T_c−Melt center temperature; T_w−Melt wall temperature; T_{coh}−Dendritic coherence temperature; t_{coh}−Dendritic coherence time): (a) *x*=0; (b) *x*=1; (c) *x*=2; (d) *x*=3

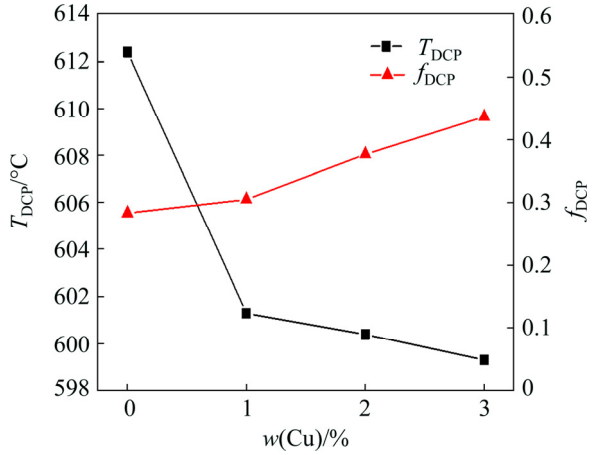

Fig. 7 Temperatures (T_{DCP}) and solid fractions (f_{DCP}) of Mg−7Zn−*x*Cu−0.6Zr alloys at coherency point

be observed at the onset of solidification. For the Mg−7Zn−0.6Zr alloy, as solidification proceeded, the force curve slope firstly increased, stabilized for a while and increased again. The force drop or stabilization indicated that hot tearing occurred during casting. The temperature corresponding to the beginning of the force drop or stabilization was considered as the hot tearing initiation temperature. In this case, the hot tearing of Mg−7Zn−0.6Zr alloy was initiated at 389 °C, which corresponded to a solid fraction of 99%. In addition, the Mg−7Zn−0.6Zr alloy force curve levels lasting stabilization signified severe hot tearing (Fig. 8(a)). This was confirmed by the macrograph presented in Fig. 8(a). For the Mg−7Zn−1Cu−0.6Zr alloy, the hot tearing initiated at 413 °C, which corresponded to the solid fraction of 93% (Fig. 8(b)). Unlike the aforementioned two alloys, the Mg−7Zn−2Cu−0.6Zr and Mg−7Zn−3Cu−0.6Zr alloy force curves did not present any clear sign of drop or stabilization. Through the macrograph observation, as indicated in Figs. 8(c) and (d), only low amount of hot tearing occurred in these two alloys.

The hot tearing volumes of Mg−7Zn−*x*Cu−0.6Zr alloys through the wax penetration method are shown in Fig. 9. It could be observed that the crack volumes were significantly reduced with the addition of Cu. The Mg−7Zn−0.6Zr alloy broke completely and was marked as "∞" in Fig. 9. The hot tearing crack volumes of the Mg−7Zn−1Cu−0.6Zr, Mg−7Zn−2Cu−0.6Zr and Mg−7Zn−3Cu−0.6Zr alloys were 134.2, 36.0 and 28.7 mm^3, respectively, being lower compared to that of the Mg−7Zn−0.6Zr alloy (Fig. 9). This implied that the hot tearing resistance of the Cu-containing alloys clearly increased.

3.4 Fracture surfaces

Figure 10 shows the hot tearing fracture surfaces of the Mg−7Zn−*x*Cu−0.6Zr alloys at the mold temperature of 250 °C. The hot tearing fracture surface of the

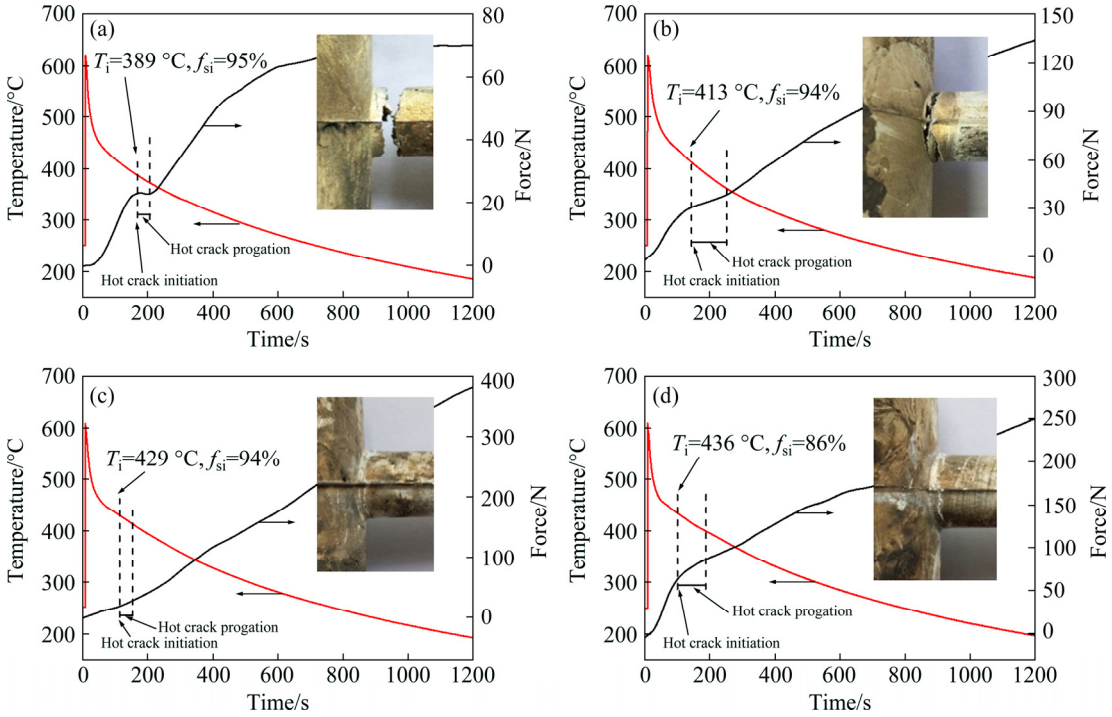

Fig. 8 Contraction force and temperature as function of solidification time at mold temperature of 250 °C for as-cast Mg−7Zn−*x*Cu−0.6Zr alloys (T_i−Hot tearing initiation temperature; f_{si}−Solid fraction at hot tearing initiation): (a) *x*=0; (b) *x*=1; (c) *x*=2; (d) *x*=3

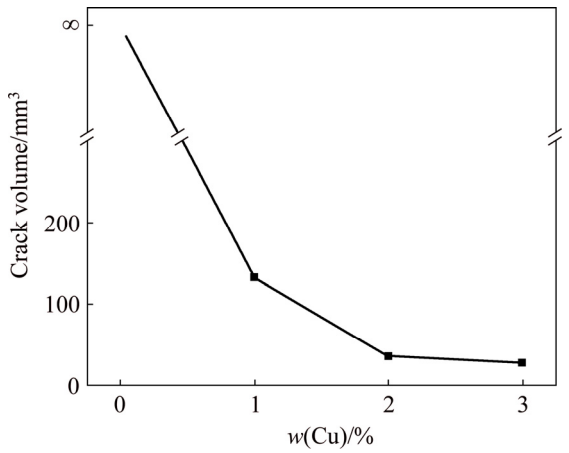

Fig. 9 Hot crack volumes of Mg−7Zn−*x*Cu−0.6Zr alloy with different Cu contents

Mg−7Zn−0.6Zr alloy was significantly clean and smooth. Also, some dendrite-like bumps were observed on the fracture surface. These dendrite-like bumps on the fracture surface indicated that the hot tearing occurred through an inter-dendritic separation in the mushy zone during solidification (Fig. 10(a)). As the Cu content increased, a low melting point phase was observed between the dendrite-like bumps. The amount of low melting point phase increased as the Cu content increased (Figs. 10(b−d)). The low melting point phase was a eutectic phase, mainly enriched with Zn and Cu, according to the EDS analysis.

4 Discussion

Hot tearing constitutes a defect occurring in the mushy zone of an alloy freezing. At the beginning of solidification, the melt temperature was between the liquidus and the dendrite coherency point temperature. In this stage, the liquid and the solid move freely. As the solidification temperature decreased, the melt temperature reached the dendrite coherency point temperature. During this stage, the dendrites started to form a solid skeleton and the liquid flowed throughout the dendrite networks. According to the solidification shrinkage compensation theory, the liquid flow was blocked and could not proceed when the dendrites formed a continuous network structure. Therefore, the hot tearing might occur. At the end of solidification, the ingot developed considerable strength and the solid state creep compensated any further contraction [3]. Normally, fine equiaxed grains would mainly occur when the dendrite coherency would form at the high solid fraction and low temperature during solidification. In contrast, a coarsened columnar grain structure was dominant when the dendrite coherency formed at low solid fraction and high temperature during solidification [20]. As an example, as shown in Fig. 7, the T_{DCP} for the Mg−7Zn−0.6Zr alloy occurred at the high temperature of 612 °C, which corresponded to the f_{DCP} of 28.3%. The microstructure of Mg−7Zn−0.6Zr alloy consisted of coarse grains, as presented in Fig. 4(b). Adversely, as the

Cu content increased, the T_{DCP} decreased from 612 to 599 °C and the f_{DCP} increased from 28.3% to 43.7%. This meant that the grain size decreased as the Cu content increased, which agreed well with the microstructural observations (as presented in Figs. 4(f) and (h)). The coarsened and columnar microstructures easily promoted the initiation and propagation of hot tearing [20]. Therefore, the Mg−7Zn−0.6Zr alloy had high HTS, which agreed well with the macrograph observations. On the contrary, the alloy with a fine and equiaxed grain structure had high hot tearing resistance. It was reasonable that the finer grains could easily accommodate the deformation caused by thermal contraction [2]. Furthermore, the eutectic phase presence at the grain boundaries with a finer grain structure allowed the free movement of the grains to accommodate the local strains without defects occurrence [21,22]. Consequently, the HTS of the Mg−7Zn−*x*Cu−0.6Zr alloys decreased as the Cu content increased.

The amount and temperature of eutectic liquid were also considered as the most important factors to affect hot tearing. Figure 11 presents the typical microstructures of the longitudinal sections for the Mg−7Zn−*x*Cu−0.6Zr alloys. The samples were cut from the region

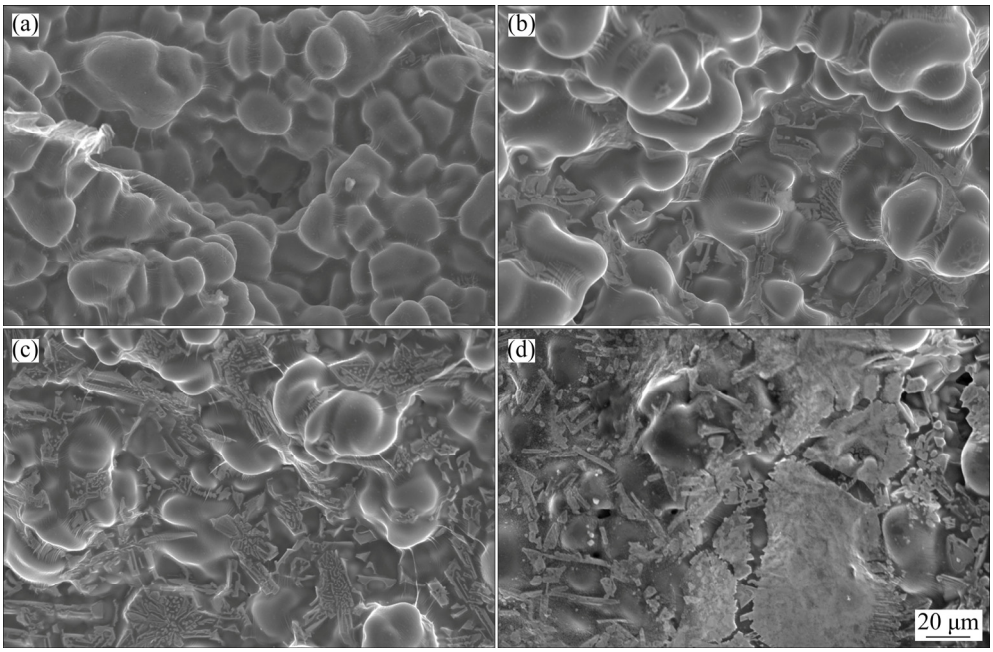

Fig. 10 Fracture surfaces of hot tearing regions for Mg−7Zn−*x*Cu−0.6Zr alloys at mold temperature of 250 °C: (a) *x*=0; (b) *x*=1; (c) *x*=2; (d) *x*=3

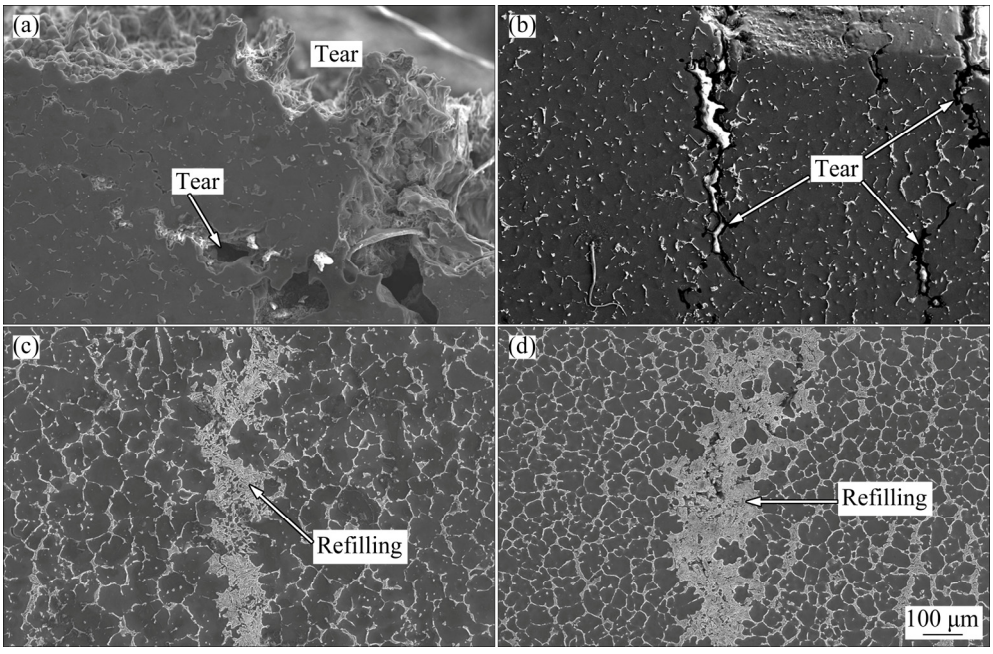

Fig. 11 Microstructures near tear region of Mg−7Zn−*x*Cu−0.6Zr alloys: (a) *x*=0; (b) *x*=1; (c) *x*=2; (d) *x*=3

near the junction. Interestingly, as presented in Figs. 11(c) and (d), a certain amount of hot tearing was refilled and could be traced along the crack path in the alloys with high Cu content. It mainly contained the eutectic phase with low melting point. Negative pressure existed near the hot tearing regions following the cracks occurrence, which caused the remaining liquid to be sucked backwards and refill the hot cracks [22−26]. Figures 4(d), (f) and (h) also presented that the eutectic phase amount increased as the Cu content increased, leading to the residual liquid presenting a high fluidity.

Moreover, the HTS was proportional to the solidification range, which could be defined as the temperature range between the α-Mg and $MgZn_2$ reaction temperatures [27]. As presented in Fig. 5, the solidification range depended on the nominal compositions of the Mg−7Zn−xCu−0.6Zr alloys. This demonstrated that the α-Mg reaction temperatures of the alloys decreased as the Cu content increased, from 627 °C (Mg−7Zn−0.6Zr) to 616 °C (Mg−7Zn−3Cu−0.6Zr). Furthermore, the $MgZn_2$ reaction temperatures increased as the Cu content increased, from 423 °C (Mg−7Zn−0.6Zr) to 457 °C (Mg−7Zn−3Cu−0.6Zr). Since the addition of Cu element narrowed down the solidification temperature ranges of the Mg−7Zn−xCu−0.6Zr alloys, the HTS values were reduced as the Cu content increased, which was also in agreement with the obtained experimental results.

5 Conclusions

1) The computer-aided cooling curve analysis results of the Mg−7Zn−0.6Zr alloys revealed two distinct precipitates: α-Mg and $MgZn_2$. Three distinct precipitates were detected following Cu addition and identified as α-Mg, MgZnCu and $MgZn_2$. The precipitation temperature of α-Mg decreased and the precipitation temperatures of $MgZn_2$ and MgZnCu increased as the Cu content increased.

2) For the Mg−7Zn−xCu−0.6Zr alloys, the dendrite coherency point temperature (T_{DCP}) decreased from 612 to 599 °C, whereas the solid fraction at the dendrite coherency point (f_{DCP}) increased from 28.3% to 43.7% as the Cu content increased from 0 to 3%.

3) The experimental results demonstrated that the addition of Cu significantly decreased the hot tearing susceptibility (HTS) of the Mg−7Zn−xCu−0.6Zr alloys due to the shortened eutectic reaction temperature.

4) Two main hot tearing mechanisms were revealed for the Mg−7Zn−xCu−0.6Zr alloys: one mechanism was the inter-dendritic separation theory for the Mg−7Zn−0.6Zr and Mg−7Zn−1Cu−0.6Zr alloys; the other mechanism was the feeding theory for the Mg−7Zn−2Cu−0.6Zr and Mg−7Zn−3Cu−0.6Zr alloys.

References

[1] YAN Yun-qi, ZHANG Ting-jie, DENG Ju, ZHOU Lian. Research and development of heat resistant Mg alloys [J]. Rare Metal Materials and Engineering, 2004, 33(6): 561−565.

[2] WANG Zhi, LI Yi-zhou, WANG Feng, HUANG Yuan-ding, SONG Jiang-feng, MAO Ping-li, LIU Zheng. Hot tearing susceptibility of Mg−xZn−2Y alloys [J]. Transactions of Nonferrous Metals Society of China, 2016, 26: 3115−3122.

[3] ESKIN D G, SUYITNO, KATGERMAN L. Mechanical properties in the semi-solid state and hot tearing of aluminum alloys [J]. Progress in Materials Science, 2004, 49: 629−711.

[4] FARAHANY S, BAKHSHESHI-RAD H R, IDRIS M H, KADIR M R A, LOTFABADI A F, OURDJINI A. In-situ thermal analysis and macroscopical characterization of Mg−xCa and Mg−0.5Ca−xZn alloy systems [J]. Thermochim Acta, 2012, 527: 180−189.

[5] EMADI D, WHITING L V, NAFISI S. Application of thermal analysis in quality control of solidification processes [J]. Journal of Thermal Analysis and Calorimetry, 2005, 81: 235−242.

[6] DOBRZANSKI L A, KROL M, TANSKI T, MANIARA R. Thermal analysis of the MCMgAl9Zn1 magnesium alloy [J]. Archives of Materials Science and Engineering, 2008, 34(2): 553−556.

[7] LIANG S M, CHEN R S, BLANDIN J J, SUERY M, HAN E H. Thermal analysis and solidification pathways of Mg−Al−Ca system alloys [J]. Materials Science and Engineering A, 2008, 480(1−2): 365−372.

[8] APELIAN D, SIGWORTH G K, WHALER K R. Assessment of grain refinement and modification of Al−Si foundry alloys by thermal analysis [J]. Transactions of the American Foundrymen's Society, 1984, 92: 297−307.

[9] MAHFOUD M, RAO A K P, EMADI D. The role of thermal analysis in detecting impurity levels during aluminum recycling [J]. Journal of Thermal Analysis and Calorimetry, 2010, 100(3): 847−851.

[10] LU L, DAHLE A K. Effects of combined additions of Sr and AlTiB grain refiners in hypoeutectic Al−Si foundry alloys [J]. Materials Science and Engineering A, 2006, 435(4): 288−296.

[11] HUANG Zhang-hong, LIANG Song-mao, CHEN Rong-shi, HAN En-hou. Solidification pathways and constituent phase of Mg−Zn−Y−Zr alloys [J]. Journal of Alloys and Compounds, 2009, 468(1−2): 170−178.

[12] CLYNE T W, DAVIES G J. The influence of composition on solidification cracking susceptibility in binary alloy systems [J]. The British Foundryman, 1981, 74: 65−73.

[13] GUNDE P, SCHIFFL A, UGGOWITZER P J. Influence of yttrium additions on the hot tearing susceptibility of magnesium−zinc alloys [J]. Materials Science and Engineering A, 2010, 527(26): 7074−7079.

[14] ZHOU L, HUANG Y D, MAO P L, KAINER K U, LIU Z, HORT N. Influence of composition on hot tearing in binary Mg−Zn alloys [J]. International Journal of Cast Metals Research, 2011, 24(3−4): 170−176.

[15] ZHU H M, SHA G, LIU J W, WU C L, LUO C P, LIU Z W, ZHENG R K, RINGER S P. Microstructure and mechanical properties of Mg−6Zn−xCu−0.6Zr(wt.%) alloys [J]. Journal of Alloys and Compounds, 2011, 509(8): 3526−3531.

[16] BUHA J, OHKUBO T. Natural aging in Mg−Zn(−Cu) alloys [J]. Metallurgical and Materials Transactions A, 2008, 39(9): 2259−2273.

[17] BACKERUD L, CHAI G, TAMMINEN J. Solidification characteristics of aluminum alloys [J]. Foundry Alloys, 1990, 2: 74−78.

[18] ZHEN Z, HORT N, HUANG Y D, NICOLAI P, OLIVER U, KARL U K. Quantitative determination on hot tearing in Mg−Al binary alloys [J]. Mater Science Forum, 2009, 618−619: 533−540.
[19] ZHANG Zhen-yan, PENG Li-ming, ZENG Xiao-qin, DING Wen-jiang. Effects of Cu and Mn on the mechanical properties and damping capacity of Mg−Cu−Mn alloy [J]. Transactions of Nonferrous Metals Society of China, 2008, 18(S_1): s55−s58.
[20] HOU Dan-hui. Solidification path, dendrite growth restriction factor and grain size of cast Mg−Al−Zn alloy [D]. Dalian: Dalian University of Technology, 2015. (in Chinese)
[21] BIRRU A K, KARUNAKAR D B. Effects of grain refinement and residual elements on hot tearing of A731 aluminium cast alloy [J]. Transactions of Nonferrous Metals Society of China, 2016, 26(7): 1783−1790.
[22] SONG J F, WANG Z, HUANG Y D, SRINIVASAN A, BECKMANN F, KARL U K. Hot tearing characteristics of Mg−2Ca−*x*Zn alloys [J]. Journal of Materials Science, 2016, 51(5): 2687−2704.
[23] ZHEN Z S, HORT N, UTKE O, HUANG Y D, PETRI N, KAINER K U. Investigations on hot tearing of Mg-Al binary alloys by using a new quantitative method [C]// Magnesium Technology 2009. San Francisco: The Minerals, Metals and Materials Society, 2009: 105−110.
[24] FARUP I, DREZET J M, RAPPAZ M. In situ observation of hot tearing formation in succinonitrile−acetone [J]. Acta Materialia, 2001, 49(7): 1261−1269.
[25] LIN S, ALIRAVCI C, PEKGULERYUZ N I O. Hot-tear susceptibility of aluminum wrought alloys and the effect of grain refining [J]. Metallurgical and Materials Transactions A, 2007, 38(5): 1056−1068.
[26] ESKIN D G, SUYITNO, MOONEY J F, KATGERMAN L. Contraction of aluminum alloys during and after solidification [J]. Metallurgical and Materials Transactions A, 2004, 35(4): 1325−1335.
[27] LIU Zheng, ZHANG Si-bo, MAO Ping-li, WANG Feng. Effects of Y on hot tearing susceptibility of Mg−Zn−Y−Zr alloys [J]. Transactions of Nonferrous Metals Society of China, 2014, 24(4): 907−914.

Mg−7Zn−*x*Cu−0.6Zr 合金的热裂行为及热分析测试

王 志[1]，周 野[1]，李一洲[1]，王 峰[1]，刘 正[1]，毛萍莉[1]，蒋小平[2]

1. 沈阳工业大学 材料科学与工程学院，沈阳 110870；
2. 万丰奥特控股集团有限公司，绍兴 312000

摘 要：通过热分析方法研究 Mg−7Zn−*x*Cu−0.6Zr 合金在凝固过程中的显微组织演变。采用具有测力传感器和数据采集系统的约束棒实验装置研究 Cu 含量(0, 1, 2 和 3，质量分数，%)对 Mg−7Zn−*x*Cu−0.6Zr 合金热裂行为的影响。Mg−7Zn−*x*Cu−0.6Zr 合金的热分析结果表明，该合金主要由 *α*-Mg 和 $MgZn_2$ 相组成，而含 Cu 合金有 3 个潜热释放峰，分别对应 *α*-Mg、MgZnCu 和 $MgZn_2$ 相。同时，随着 Cu 含量的增加，*α*-Mg 相的反应温度降低，$MgZn_2$ 和 MgZnCu 相的反应温度升高。热裂实验结果表明，由于添加 Cu 能提高合金的共晶温度，而缩小凝固温度区间，因此，Mg−7Zn−*x*Cu−0.6Zr 合金的热裂敏感性明显降低。

关键词：Mg−7Zn−*x*Cu−0.6Zr 合金；显微组织；凝固路径；热裂敏感性

(Edited by Wei-ping CHEN)